Journal of ELECTRONIC MATERIALS, Vol. 45, No. 4, 2016
DOI: 10.1007/s11664-015-4278-3
© 2015 The Minerals, Metals & Materials Society

# Temperature Dependence and High-Temperature Stability of the Annealed Ni/Au Ohmic Contact to *p*-Type GaN in Air

SHIRONG ZHAO,[1,4] HEATHER MCFAVILEN,[2] SHUO WANG,[3] FERNANDO A. PONCE,[3] CHANTAL ARENA,[2] STEPHEN GOODNICK,[1] and SRABANTI CHOWDHURY[1]

1.—School of Electrical, Computer and Energy Engineering, Arizona State University, Tempe, AZ 85287, USA. 2.—Soitec Phoenix Labs, Tempe, AZ 85284, USA. 3.—Department of Physics, Arizona State University, Tempe, AZ 85287, USA. 4.—e-mail: shirong.zhao@asu.edu

We report on the temperature-dependent contact resistivity and high-temperature stability of the annealed Ni/Au ohmic contacts to *p*-type GaN in air. As the measure temperature increases from 25°C to 390°C, both the specific contact resistivity ($\rho_c$) and sheet resistance ($R_{sh}$) decrease by factors ~10, contributing to the 10-fold increase in current at 390°C compared with that at 25°C. It was also observed that the $\rho_c$ was further reduced by 36%, i.e., from $2.2 \times 10^{-3}\ \Omega\ cm^2$ to $1.4 \times 10^{-3}\ \Omega\ cm^2$, during the 48-h high-temperature stability test at 450°C in air, showing excellent stability of the contacts. An increase in $\rho_c$ was observed after the contacts were subjected to 500°C in air. Higher temperature stress led to a significant increase in $\rho_c$. The contacts show rectifying I–V characteristics after being subjected to 700°C for 1 h. The degradation mechanics were analyzed with the assistance of transmission electron microscopy and energy dispersive x-ray spectroscopy.

**Key words:** Ni/Au ohmic contacts, *p*-type GaN, specific contact resistivity, high-temperature electronics

## INTRODUCTION

Many industries, including automobiles, aircrafts, gas turbines, oil exploration, and space exploration, require electronics that can operate reliably at high temperatures.[1–5] Traditionally, engineers rely on active or passive cooling when designing electronics that must function above typical high (150°C) temperature ranges. However, active cooling is not always a desired option in many applications or the cost can be very high. Electronics that can operate under high temperature are, therefore, required to improve the system reliability and reduce cooling and, hence, overall system cost. Conventional silicon devices cannot be operated reliably above 150°C due to the generation of thermal carriers which can cause leakage and latch-up at reverse bias.[1] GaN-based technology is attractive for harsh environment operation because of its high chemical and physical stability; GaN has a higher atomic displacement energy than many other semiconductor materials. It was reported that the practical temperature limit of GaN is 600°C,[2] sufficient to support long-term device operation at high temperature. The high thermal stability of GaN is advantageous for many high-temperature applications such as power electronics, and in designing high-temperature, GaN-based hybrid solar cells, for application in concentrated solar thermal converters. Such hybrid solar cell/concentrating solar thermal systems have the potential for much higher energy conversion efficiency when operating at elevated temperatures.[6,7] One challenge in the realization of a reliable hybrid solar cell for high-temperature operation is to achieve stable metal contacts to the semiconductor. At temperatures higher than 200°C, failure of the entire cell can occur due to the diffusion of the contact metals, oxidation and reactions at the metal–semiconductor interface at high temperatures, even

(Received August 22, 2015; accepted December 1, 2015; published online December 29, 2015)

though the intrinsic GaN cell remains stable and maintains a good efficiency. Therefore, the development of thermally and electrically stable ohmic contacts for high-temperature operation is critical for high-temperature electronics, including hybrid solar cells.

The focus of this work was specifically derived from the purpose of achieving appropriate metal contacts to the high-temperature InGaN solar cell, which will be integrated with a concentrating solar thermal power module. The hybrid (solar + heat) system operates at an efficiency of 55% when operated at 450°C, much higher than the current world record of solar cell efficiency. It is clear from the overall system efficiency of such application that we are relying on high-temperature operation of InGaN solar cells with an optimum efficiency. An InGaN solar cell operating at temperatures in excess of 300°C requires thermally stable contacts to both *n*-type GaN and *p*-type GaN capping layers. Hou et al. reported that alloyed Ti/Al/Pt/Au to *n*-type GaN contacts were very stable at 600°C over 10 h in an oxidizing air ambient.[8] The temperature dependence of the specific contact resistivity in Ti/Al/Ni/Au ohmic contacts to *n*-GaN has been studied as well.[9,10] In this report we will focus on the ohmic contacts to *p*-type GaN at elevated temperatures. Ni/Au double layer contact technology to form ohmic contacts to *p*-type GaN at room temperature has been widely reported.[11–16] However, their performance at high temperature (above 300°C), maximum thermal limits of operation and possible failure mechanisms remain largely unexplored. In this paper, we report our observation of the temperature-dependent contact resistivity and high-temperature stability of the annealed Ni/Au ohmic contacts to *p*-type GaN.

## EXPERIMENTAL

The *p*-type GaN epitaxial layers were grown by metal organic chemical vapor deposition (MOCVD). An unintentionally doped *c*-plane GaN buffer layer (3.1 $\mu$m) was first grown on sapphire substrate, followed by 300-nm thick *n*-type GaN with a Si doping concentration of $1 \times 10^{17}$ cm$^{-3}$ and 100-nm thick *p*-type GaN with a Mg doping concentration of $3 \times 10^{19}$ cm$^{-3}$. The structure was capped with 10 nm of $p^+$GaN with a Mg doping concentration of $1 \times 10^{20}$ cm$^{-3}$.

The determination of the specific contact resistivity ($\rho_c$) and sheet resistance ($R_{sh}$) were carried out by the transmission line method (TLM).[17] Mesa regions for TLM measurements were defined using inductively coupled plasma (ICP) etching to etch down to the *n*-type GaN. Ni/Au (20/200 nm) TLM contact pads, with an area of $100 \times 200$ $\mu$m$^2$, were deposited using e-beam evaporation. A 1-min dip in HCl:DI water (1:3) mixture was conducted to remove the native oxide layers prior to e-beam evaporation of the contact pads. After deposition and lift-off of the Ni/Au contacts, we subjected the samples to a rapid thermal annealing (RTA) process at 500°C, 550°C, and 600°C in a $N_2$ ambient for various time intervals ranging from 2 min to 10 min. The current–voltage (*I–V*) characteristics of the annealed contacts were measured using a four-point probe station equipped with a Keithley semiconductor characterization system (4200-SCS) parameter analyzer. The contacts formed by RTA at 600°C for 3 min showed the lowest specific contact resistivity, $\rho_c$, $1.6 \times 10^{-3}$ Ω cm$^2$, with a sheet resistance, $R_{sh}$ , of $1.3 \times 10^5$ Ω/□. $\rho_c$ and $R_{sh}$ were extracted from the linear plot of measured resistance ($R_{measured}$) versus contact pad spacing, shown in Fig. 1, according to the TLM model. The linear *I–V* curves of the optimized contacts are shown in the graph inset of Fig. 1, depicting very good ohmic behavior at room temperature (25°C).

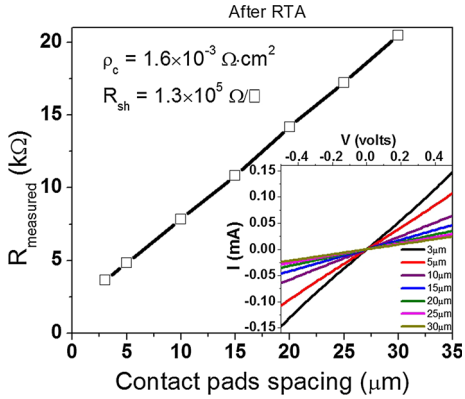


Fig. 1. Measured resistance versus TLM pad spacing after the Ni/Au to *p*-GaN contacts were annealed at 600°C in $N_2$ for 3 min. The insert graph shows the *I–V* curves measured between adjacent contact pads with various spacing.

The temperature dependence of the specific contact resistivity and sheet resistance were studied in the range of 25–390°C, varying the chuck temperature by using an Instec mK2000 temperature controller. The thermal stability of the annealed Ni/Au to *p*-GaN contacts was tested on another sample, with average initial $\rho_c$ of $2.2 \times 10^{-3}$ Ω cm$^2$, in a Minibrute furnace at 450°C with ambient air for a maximum of 48 h, during which time the test sample was taken out of the furnace and the *I–V* characteristics were measured at room temperature at regular intervals. To identify the high-temperature limit of the contacts, the test sample was then subjected to thermal stress at 500°C, 550°C, 600°C, 650°C, and 700°C in series in the Minibrute furnace with ambient air. *I–V* characteristics were measured at room temperature after each thermal stress and the specific contact resistivity was extracted. The contacts degradation mechanism was studied by transmission electron microscopy (TEM) and *in situ* energy dispersive x-ray analysis (EDX).

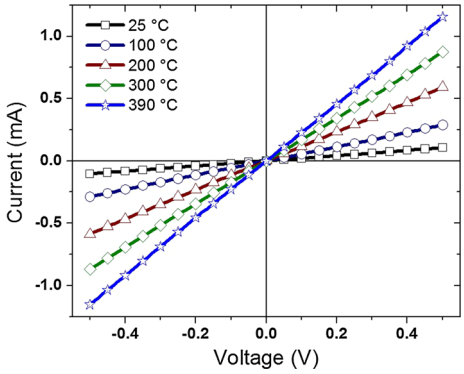


Fig. 2. Temperature-dependent *I–V* characteristics of the annealed contacts, taken between two adjacent pads with a gap spacing of 5um.

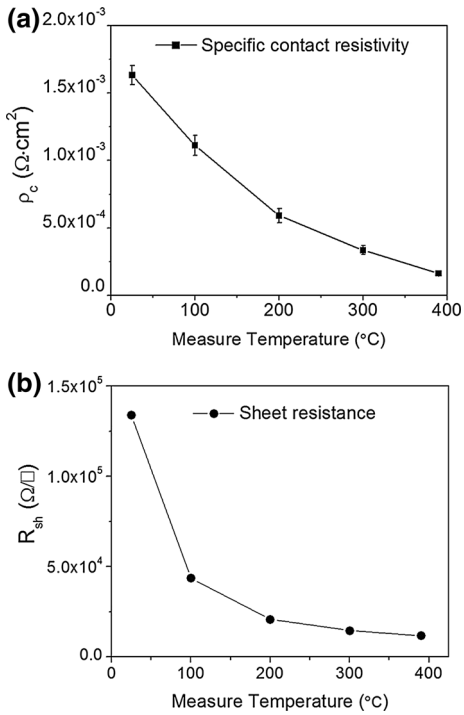


Fig. 3. Specific contact resistivity $\rho_c$ (a) and sheet resistance $R_{sh}$ (b) as a function of the measure temperature.

## RESULTS AND DISCUSSION

### Dependence of $\rho_c$ and $R_{sh}$ on Temperatures up to 390°C

Figure 2 shows the *I–V* characteristics of the contacts measured at various temperatures between 25°C and 390°C taken between two adjacent TLM pads with a gap spacing of 5 $\mu$m. The contacts remain ohmic at all temperatures from 25°C to 390°C and the current increases with the increasing measure temperature. The current at 390°C is 10 times higher than that at 25°C. The $\rho_c$ and $R_{sh}$ values of the contacts, extracted from the TLM measurements, as a function of the measure temperature are shown in Fig. 3a and b, respectively.

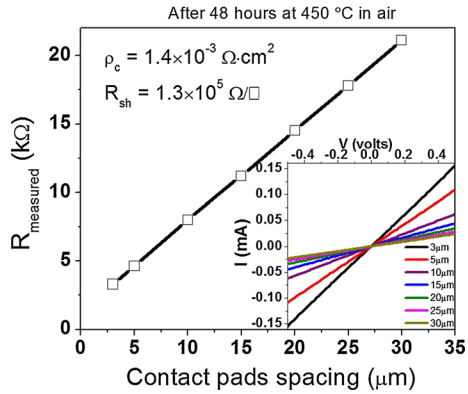


Fig. 4. Measured resistance versus TLM pad spacing after the contacts samples were subjected to 450°C in air for 48 h. The insert graph shows the *I–V* curves measured between contact pads with various spacing.

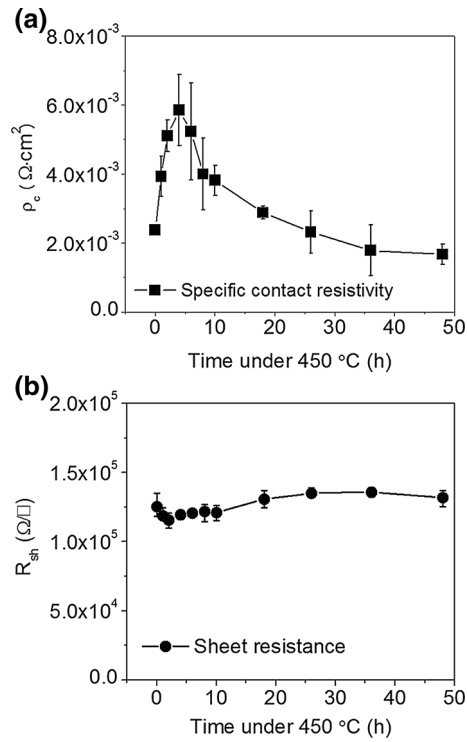


Fig. 5. Time evolution of the specific contact resistivity $\rho_c$ (a) and sheet resistance $R_{sh}$ (b) over the 48-h thermal stability test at 450°C in air.

Both specific contact resistivity and sheet resistance decrease with increasing measure temperature. $\rho_c$ decreases by a factor of 10, i.e., from $1.6 \times 10^{-3}$ $\Omega$ cm$^2$ at 25°C to $1.6 \times 10^{-4}$ $\Omega$ cm$^2$ at 390°C. $R_{sh}$ decreases by a factor of 11, i.e., from $1.3 \times 10^5$ $\Omega/\square$ at 25°C to $1.2 \times 10^4$ $\Omega/\square$ at 390°C. The reduction in $\rho_c$ and $R_{sh}$ is probably due to the increased hole concentration at high temperature,[18] and it is responsible for the increase in current. Therefore, the contacts shows superior ohmic behavior at elevated temperatures.

### Stability of the Contacts at 450°C in Air

Figure 4 shows the plot of measured resistance versus contact pad spacing after the sample was subjected to 450°C in an ambient of air for 48 h. The *I–V* curves obtained after the 48-h high-temperature test, as shown in the inset of Fig. 4, validate that the contacts maintain very good ohmic behavior. The $\rho_c$ and $R_{sh}$ extracted from Fig. 4 are $1.4 \times 10^{-3}$ Ω cm$^2$ and $1.32 \times 10^5$ Ω/□, respectively. The change in $\rho_c$ and $R_{sh}$, compared with those before the high-temperature test, are approximately −36% and 6%, respectively. The improvement in the $\rho_c$ was possibly a result of further annealing of the contacts, although the possibility of typical errors incurred in the TLM method cannot be ruled out.[19]

Figure 5a shows the time evolution of the specific contact resistivity measured and averaged over multiple TLM structures when held at 450°C in air. A significant increase and then decrease in $\rho_c$ was observed during the initial 10-h "burn-in" period.[8] After 10 h, the $\rho_c$ decreased slowly and stabilized at $\sim 2 \times 10^{-3}$ Ω cm$^2$. No degradation was observed, thereby demonstrating excellent thermal stability of these contacts at 450°C in air. Figure 5b shows the time evolution of the sheet resistance at 450°C in air, obtained from the same TLM readings. The change in $R_{sh}$ is negligible, as expected, since 450°C is far below the dissociation temperature

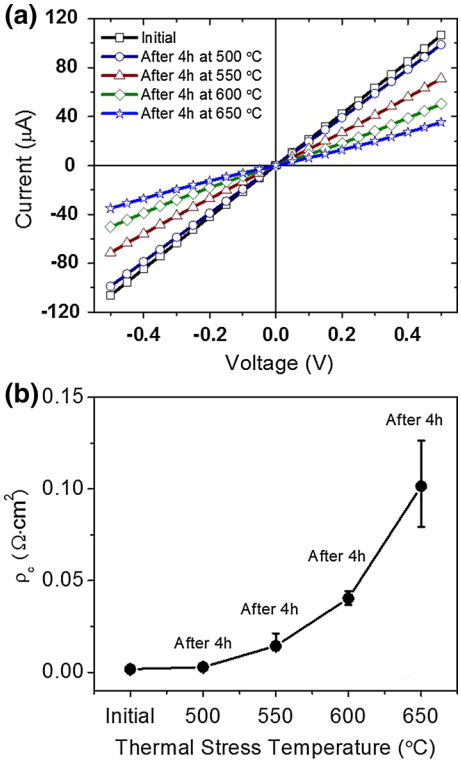


Fig. 6. (a) *I–V* characteristics measured at room temperature and taken between two adjacent TLM pads with a gap spacing of 5 μm and (b) the extracted $\rho_c$ of the contacts after being subjected to thermal stress above 450°C in air.

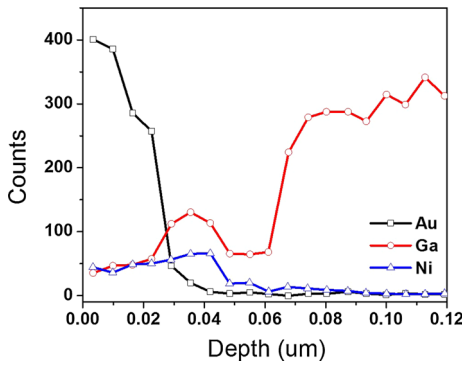


Fig. 8. EDS of the *p*-type GaN surface with cracks after being subjected to 700°C in air for 1 h.

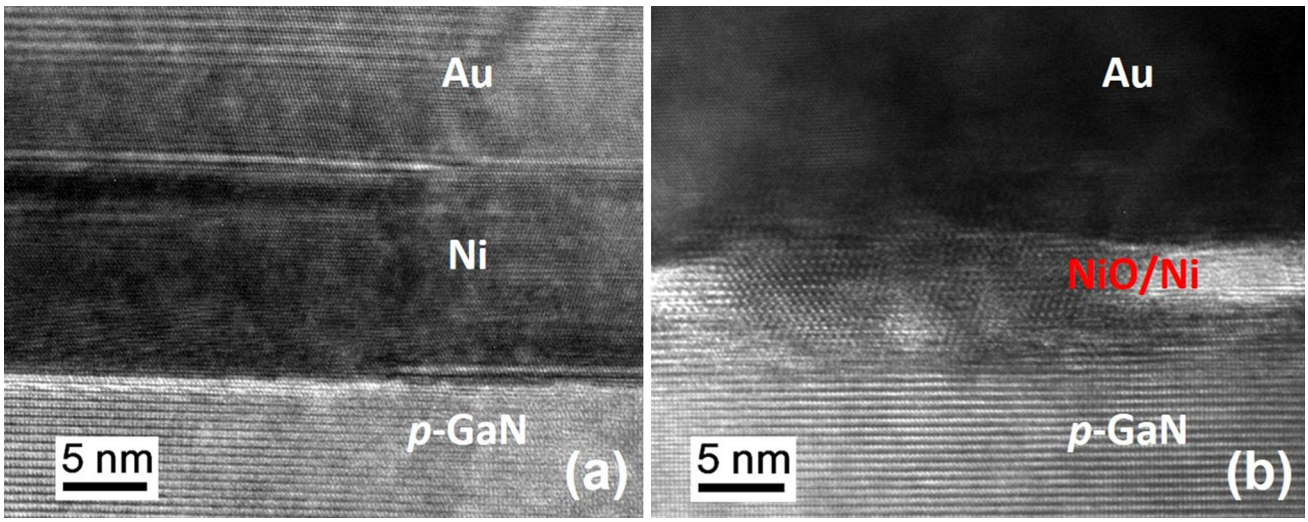


Fig. 7. Comparison of the TEM images on the metal–semiconductor interface between sample (a) Ni/Au contacts baked at 450°C and sample (b) Ni/Au contacts baked at 700°C in air for 1 h.

limit of GaN.[2,20] The measurements were repeated for multiple TLM structures across the sample and the results were consistent, showing excellent stability of our contact process.

### Contacts Degradation Above 450°C

In an effort to identify the high-temperature limits of operation, the above sample was further subjected to higher temperatures from 500°C to 700°C in the Minibrute furnace with ambient air. Figure 6a shows the *I–V* characteristics of the contacts, measured at room temperature and taken between two adjacent TLM pads with a gap spacing of 5 $\mu$m before and after thermal stress at temperatures above 450°C. The *I–V* curves remain linear even after thermal stress at 650°C for 4 h, but the current is significantly reduced as the temperature increases to 650°C. Figure 6b shows the evolution of the specific contact resistivity caused by the thermal stress at temperatures above 450°C. $\rho_c$ increases by 69% after 4 h of thermal stress at 500°C, further increasing by 400% after 4 h of thermal stress at 550°C, by 180% after 4 h of thermal stress at 600°C, and by 152% after 4 h of thermal stress at 650°C. The contacts showed rectifying *I–V* curves (not shown) after being subjected to 700°C with ambient air for 1 h and the current was reduced by 3 orders of magnitude compared to the initial value.

In order to understand the root cause of such electrical behavior, we performed TEM studies on the metal–semiconductor interface of the contacts. Figure 7 shows the comparison of TEM images obtained from the two samples that were subjected to long-term bakes at 450°C, showing good ohmic behavior, and at 700°C, showing rectifying *I–V* characteristics. The metal–semiconductor interface of the 450°C-baked sample shown in Fig. 7a maintained good integrity while the 700°C-baked sample showed voids on the interface as well as dislocations starting from the surface of the *p*-type GaN, shown in Fig. 7b. The heat treatment at 700°C for 1 h also caused cracks near the *p*-type GaN surface. Energy dispersive x-ray spectroscopy (EDS) shows that the cracks have more Ni than the rest of the unbroken *p*-type GaN surface (Fig. 8), indicating the diffusion of Ni into *p*-GaN. The TEM image (Fig. 7b) shows the possible formation of NiO at the interface, which is believed to be the reason behind the degraded contact resistance.

## CONCLUSIONS

In conclusion, we have performed the temperature-dependent study of the annealed Ni/Au contacts to *p*-type GaN, depicting reduced specific contact resistivity and sheet resistance at elevated temperatures. We have also demonstrated excellent high-temperature stability of the Ni/Au contacts, surviving over 48 h at 450°C in air, showing no degradation of contact resistivity. During this period of high-temperature treatment, a stable resistivity of $\sim 2 \times 10^{-3}\ \Omega\ \mathrm{cm}^2$ was measured at regular intervals using TLM structures over multiple samples. The impressive results discussed in this paper demonstrate very stable contact performance and make GaN a material of choice for hybrid solar cell technology.

## ACKNOWLEDGEMENTS

The work presented herein was funded in part by the Advanced Research Projects Agency-Energy (ARPA-E), U.S. Department of Energy, under award number DE-AR0000470.

## REFERENCES

1. P.G. Neudeck, R.S. Okojie, and L.-Y. Chen, *Proc. IEEE* 90, 1065 (2002).
2. H.A. Mantooth, M.M. Mojarradi, and R.W. Johnson, *IEEE Power Electron. Soc. Newslett.* 18, 9 (2006).
3. R.W. Johnson, J.L. Evans, P. Jacobsen, J.R. Thompson, and M. Christopher, *IEEE Trans. Electron. Packag. Manuf.* 27, 164 (2004).
4. W.J. Pulliam, P.M. Russler, and R.S. Fielder, *Proc. SPIE* 4578, 229 (2002).
5. T. George, K.-A. Son, R.A. Powers, L.Y. Del Castillo, and R. Okojie, *2005 IEEE Sensors* (2005).
6. A. Luque and A. Martí*Sol. Energy Mater. Sol. Cells* 58, 147 (1999).
7. Y. Yang, W. Yang, W. Tang, and C. Sun, *Appl. Phys. Lett.* 103, 083902 (2013).
8. M. Hou and D.G. Senesky, *Appl. Phys. Lett.* 105, 081905 (2014).
9. F. Lin, B. Shen, S. Huang, F.J. Xu, L. Lu, J. Song, F.H. Mei, N. Ma, Z.X. Qin, and G.Y. Zhang, *J. Appl. Phys.* 105, 093702 (2009).
10. F. Iucolano, F. Roccaforte, A. Alberti, C. Bongiorno, S.D. Franco, and V. Raineri, *J. Appl. Phys.* 100, 123706 (2006).
11. J.K. Sheu, Y.K. Su, G.C. Chi, P.L. Koh, M.J. Jou, C.M. Chang, C.C. Liu, and W.C. Hung, *Appl. Phys. Lett.* 74, 2340 (1999).
12. J.-K. Ho, C.-S. Jong, C.C. Chiu, C.-N. Huang, C.-Y. Chen, and K.-K. Shih, *Appl. Phys. Lett.* 74, 1275 (1999).
13. J.-K. Ho, C.-S. Jong, C.C. Chiu, C.-N. Huang, K.-K. Shih, L.-C. Chen, F.-R. Chen, and J.-J. Kai, *J. Appl. Phys.* 86, 4491 (1999).
14. L.-C. Chen, J.-K. Ho, C.-S. Jong, C.C. Chiu, K.-K. Shih, F.-R. Chen, J.-J. Kai, and L. Chang, *Appl. Phys. Lett.* 76, 3703 (2000).
15. S. Zhao, Y. Shi, H. Li, and Q. He, *Nucl. Instrum. Methods Phys. Res. Sect. B* 268, 1435 (2010).
16. H. Omiya, F.A. Ponce, H. Marui, S. Tanaka, and T. Mukai, *Appl. Phys. Lett.* 85, 6143 (2004).
17. G.K. Reeves and H.B. Harrison, *IEEE Electron Device Lett.* 3, 111 (1982).
18. D. Steigerwald, S. Rudaz, H. Liu, R.S. Kern, W. Götz, and R. Fletcher, *JOM* 49, 18 (1997).
19. D. Sawdai, D. Pavlidis, and D. Cui, *IEEE Trans. Electron Devices* 46, 1302 (1999).
20. I. Daumiller, C. Kirchner, M. Kamp, K.J. Ebeling, and E. Kohn, *IEEE Electron Device Lett.* 20, 448 (1999).